# Ageostrophic Geopotential Fluxes in Downstream and Upstream Development of Baroclinic Waves

ISIDORO ORLANSKI AND EDMUND K. M. CHANG*

*Geophysical Fluid Dynamics Laboratory/NOAA, Princeton University, Princeton, New Jersey*

(Manuscript received 15 August 1991, in final form 1 April 1992)

ABSTRACT

With the use of a simple primitive equation model, it is demonstrated that the convergence/divergence of ageostrophic geopotential fluxes can be a major source/sink of kinetic energy for both downstream and upstream development of baroclinic waves, and can play a dominant role during the early stages of wave development. It is also shown that both surface friction and $\beta$ effects lead to an asymmetry in the upstream versus downstream development, with downstream development much stronger. A total group velocity is defined based on ageostrophic fluxes, and its relationship to the rate of wave packet spreading and to convective and absolute instability is discussed.

## 1. Introduction

Recently, Orlanski and Katzfey (1991, hereafter OK) examined the life cycle of a strong cyclone that developed over the South Pacific in early September 1987. It was found that the downstream dispersion of energy by the ageostrophic geopotential fluxes was the primary reason that the cyclone ceased to grow, and that the energy transported downstream acted as a triggering mechanism for the growth of a new downstream disturbance. This result differed significantly from those of previous studies on the life cycle of baroclinic waves. In a study of nonlinear evolution of baroclinic waves from normal-mode initial conditions, Simmons and Hoskins (1978) showed that the waves decayed primarily through transfer of eddy energy to the mean flow. However, normal-mode studies are not completely realistic in the sense that they require the simultaneous growth and decay of a number of identical waves over the globe. The complementary, and somewhat more realistic, problem of downstream development of baroclinic Rossby waves traveling as a time-dependent wave packet has received relatively less attention.

Simmons and Hoskins (1979, hereafter SH) studied the response of a baroclinically unstable atmosphere to a localized initial perturbation. They found that disturbances grew both downstream and upstream of the initial disturbance. They also found that the growth rate of the downstream disturbances was larger than that of the fastest-growing normal mode, and that the upper-level maximum of the disturbances was reached earlier than the surface maximum, from which they concluded that there might be some form of downstream dispersion of energy. However, they did not analyze the energetics of the process and did not study this energy dispersion in detail. In the present study we will concentrate on the energetics of downstream and upstream development.

In this paper, we examine further the processes involved in the local transfer of energy, particularly the role of the ageostrophic fluxes, which are shown to be important in OK, in an idealized setting using numerical simulations of a simple primitive equation model. The basic state, the initial perturbation, and the characteristics of the numerical model are described in section 2. In section 3, the eddy kinetic energy equation is derived. Section 4 presents the results of linear experiments for both the Eady case and the jet case on an $f$ plane, as well as effects of $\beta$. Nonlinear results are discussed in section 5. The relationship between energy dispersion and absolute and convective instability is presented in section 6, and the conclusions are found in section 7.

## 2. Experiment description

A numerical model has been used to study the response of two basic flows to an initial perturbation, in both linear and nonlinear simulations, and for both $f$-plane and $\beta$-plane approximations. This section describes the characteristics of the model, the basic flows

* Also Atmospheric and Oceanic Sciences Program.

*Corresponding author address:* Dr. Isidoro Orlanski, Princeton University, GFDL/NOAA, Atmospheric and Oceanic Sciences Program, Princeton, NJ 08542.

used, and the initial perturbation field. The model and the basic jet structure are similar to those used by Nakamura (1989).

### a. Numerical model

The numerical model used for this study is a simplified version of the three-dimensional primitive equation model discussed in Ross and Orlanski (1982); interested readers are referred to that paper for details. Major simplifications employed here include the neglect of moisture effects and the use of the Boussinesq approximation. The geometry of the problem is simplified by neglecting curvature effects except in terms of beta. In effect, the following equations are solved for a channel in a $\beta$ (or $f$) plane:

$$\frac{\partial \mathbf{V}}{\partial t} = -(\nabla \cdot \mathbf{V}\mathbf{V}) - \frac{\partial}{\partial z} W\mathbf{V} - c_p\Theta_0 \nabla \Pi - f\mathbf{k} \times \mathbf{V} + \left(\kappa_h \nabla^2 \mathbf{V} + \kappa_v \frac{\partial^2 \mathbf{V}}{\partial z^2}\right)$$

$$\frac{\partial \Theta}{\partial t} = -(\nabla \cdot \mathbf{V}\Theta) - \frac{\partial}{\partial z} W\Theta + \kappa_h \nabla^2 \Theta + \kappa_v \frac{\partial^2 \Theta}{\partial z^2}$$

$$\nabla \cdot \mathbf{V} + \frac{\partial W}{\partial z} = 0$$

$$C_p\Theta_0 \frac{\partial \Pi}{\partial z} = \frac{g\Theta}{\Theta_0}, \tag{2.1}$$

where $\mathbf{V}$ is the two-dimensional horizontal wind vector and $W$ the vertical velocity; $\Theta$ is the potential temperature, $\Pi$ the Exner pressure $(P/P_0)^{R/cp}$, and $\nabla$ is the two-dimensional gradient operator. We will neglect all physical processes except for a simple diffusion-parameterizing subgrid-scale dissipation. Linear and nonlinear forms of the model were used. In the linear version, quadratic terms in the perturbations from the basic state are ignored.

### b. Basic flows

Two different basic states have been used in this study. The first is that of the Eady problem (Eady 1949), in which there is no horizontal shear and the vertical shear is constant; that is, $U = U_0 + \Lambda z$ is only a function of $z$. As a slightly more realistic case, a second basic flow consisting of a baroclinic jet is used. The jet profile is given by

$$\bar{U} = \begin{bmatrix} 0, & 0 \leq y < \dfrac{L_y - L_B}{2} \\ \Lambda \dfrac{z}{2}\left\{1 - \cos\dfrac{2\pi}{L_B}\left(y - \dfrac{L_y - L_B}{2}\right)\right\}, & \dfrac{L_y - L_B}{2} \leq y \leq \dfrac{L_y + L_B}{2} \\ 0, & \dfrac{L_y + L_B}{2} < y < L_y \end{bmatrix} \tag{2.2}$$

and is illustrated in Fig. 1. For both cases, the basic-state meridional velocity $\bar{V} = 0$ and the basic-state potential temperature is defined by

$$\frac{g}{\Theta_0}\frac{\partial \bar{\Theta}}{\partial z} = N_0^2$$

$$\frac{g}{\Theta_0}\frac{\partial \bar{\Theta}}{\partial y} = -f\frac{\partial \bar{U}}{\partial z}, \tag{2.3}$$

where $N_0^2 = \text{const}$ and $f = f_0 + \beta y$; $\beta$ is taken to be zero for the $f$-plane simulations.

A grid size of 150 km and a channel length of 30 000 km is used for most of the numerical runs. For the jet case, $L_B = 6000$ km and $L_y = 15\,000$ km. For the Eady case, a total channel width of 7500 km is used. The vertical resolution is 1 km with a total height of $H = 13$ km, $\Lambda$ is taken to be 2 m s$^{-1}$ km$^{-1}$, and a Richardson number of 11 is used for all cases; $f_0$ equals 0.0001 s$^{-1}$, $\beta$ is taken to be $1 \times 10^{-11}$ m$^{-1}$ s$^{-1}$ (0 for $f$-plane cases), $\kappa_h$ is taken to be 100 000 m$^2$ s$^{-1}$, and $\kappa_v$ is zero.

### c. Initial perturbation

Although Farrell (1984) found that the initial growth of disturbances in a baroclinic flow depends critically on the form of the initial perturbation, here we are more interested in longer time ($\sim$ days) response in which the unstable modes dominate. Experiments with different initial conditions have shown that the long-term response is independent of the initial perturbation as long as it is localized. Following SH, a localized barotropic vorticity disturbance is taken as the initial perturbation. In order to reduce the effects of gravity waves, both the initial divergence of the perturbation and its time tendency are set to zero. Since the initial perturbation is assumed to be nondivergent, the velocity perturbation can be solved by

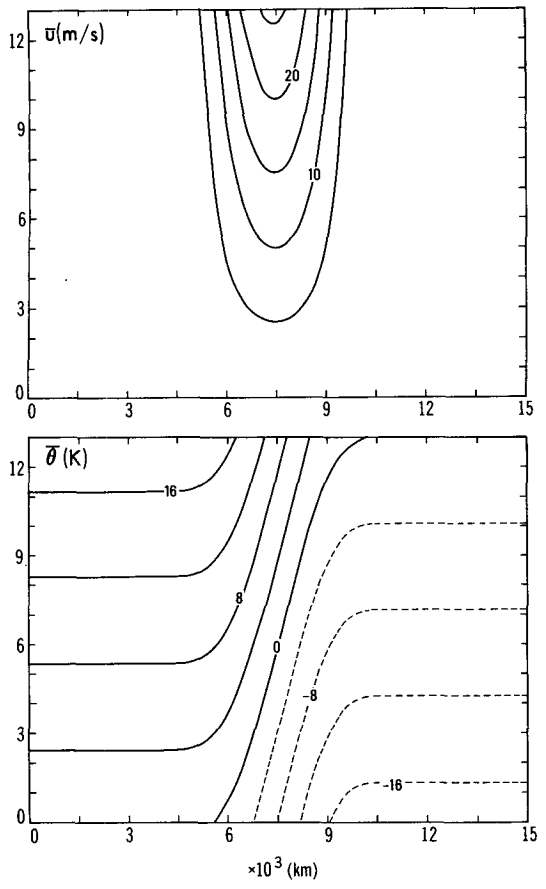


FIG. 1. Upper panel: Meridional cross section of the zonal velocity of the basic jet profile as defined by (2.2). Lower panel: Basic-state potential temperature in thermal wind balance with the zonal wind.

$$\nabla^2\psi_i = \zeta_i, \tag{2.4}$$

and

$$v_i = \frac{\partial\psi_i}{\partial x}$$

$$u_i = -\frac{\partial\psi_i}{\partial y}, \tag{2.5}$$

where $\zeta_i$ is the specified initial vorticity perturbation. In the following numerical studies, $\zeta_i$ is taken to be a Gaussian

$$\zeta_i = \zeta_0 e^{-(x^2+y^2)/d^2}, \tag{2.6}$$

where $d \sim \lambda = (N_0 H)/f_0$. The linearized equations of motion imply

$$\frac{\partial\bar{U}}{\partial y}\frac{\partial v_i}{\partial x} - f\zeta_i + \beta u_i = -C_p\Theta_0\nabla^2\pi_i. \tag{2.7}$$

Using the hydrostatic relation and remembering that the initial perturbation is constant in height, we get

$$\nabla^2\theta_i = -\frac{\Theta_0}{g}\frac{\partial^2\bar{U}}{\partial y\partial z}\frac{\partial v_i}{\partial x}. \tag{2.8}$$

For the nonlinear run, the amplitude of the perturbation is such that the maximum initial velocity perturbation approximately equals 1 m s$^{-1}$. The initial perturbation for the jet case is shown in Fig. 2. For the Eady case, the initial velocity perturbations are exactly the same, but the initial temperature perturbation is zero.

## 3. Energetics equations

To examine the evolution of the energy budget, the velocity, pressure, and temperature are separated into a mean part and a perturbation part. Bar terms below indicate the basic initial flow (described in section 2) and the lowercase letters indicate the deviation; that is,

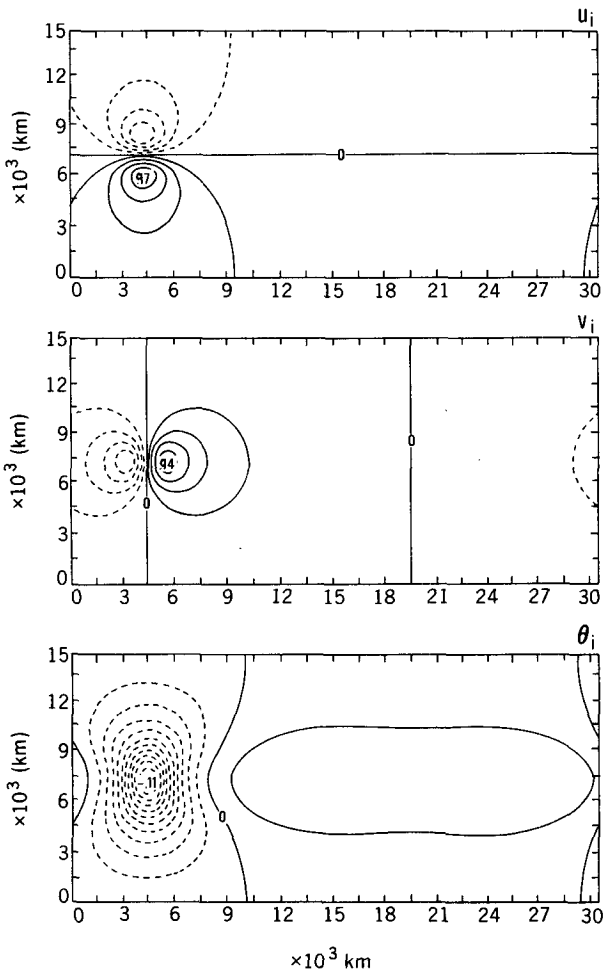


FIG. 2. Initial $u_i$, $v_i$ (m s$^{-1}$) and $\theta_i$ (deg) perturbation for the jet experiments.

$$\mathbf{V} = \bar{\mathbf{V}} + \mathbf{v}$$
$$\Pi = \bar{\Pi} + \pi$$
$$\Theta = \bar{\Theta} + \theta. \quad (3.1)$$

The same decomposition will be used for both the linear and nonlinear cases to facilitate comparison of the results. Since the mean state here is time independent, zonally symmetric, and geostrophically balanced, the momentum equation for the perturbation field becomes

$$\left(\frac{\partial}{\partial t} + \bar{\mathbf{V}}\cdot\nabla\right)\mathbf{v} + \mathbf{v}\cdot\nabla\mathbf{v} + w\frac{\partial \mathbf{v}}{\partial z} + \mathbf{v}\cdot\nabla\bar{\mathbf{V}} + w\frac{\partial}{\partial z}\bar{\mathbf{V}} + f\mathbf{k}\times\mathbf{v} = -c_p\Theta_0\nabla\pi + \text{diss}. \quad (3.2)$$

Multiplying (3.2) by $\mathbf{v}$ yields the energy equation:

$$\left(\frac{\partial}{\partial t} + \bar{\mathbf{V}}\cdot\nabla\right)K_e + \mathbf{v}_3\cdot\nabla_3 K_e = -c_p\Theta_0(\mathbf{v}\cdot\nabla\pi) - (\mathbf{v}\cdot(\mathbf{v}_3\cdot\nabla_3)\bar{\mathbf{V}}) + \text{diss}, \quad (3.3)$$

where $\nabla_3$ is the three-dimensional gradient operator and $\mathbf{v}_3$ is the three-dimensional perturbation velocity. The terms on the left are the time tendency of the eddy kinetic energy $K_e$, advection by the mean flow, and advection by the perturbation itself. For linear runs, the third term on the left-hand side will be absent. The first term on the right can be written (using continuity and hydrostatic equations):

$$-c_p\Theta_0(\mathbf{v}\cdot\nabla\pi) = -(c_p\Theta_0\nabla_3\cdot\mathbf{v}_3\pi) + g\frac{w}{\Theta_0}\theta. \quad (3.4)$$

The first term on the right-hand side is equivalent to the divergence of geopotential flux term in OK (strictly speaking, this is a pressure flux term since the model used here is in height coordinates instead of pressure coordinates. We decided, however, to continue calling it the geopotential flux term following OK in order not to use different names for essentially the same physical quantity), and the second term is the baroclinic conversion term. The second term on the right of (3.3) can be interpreted as barotropic conversion between the mean flow and the eddies.

Following OK, we write

$$\mathbf{v}_3 = \mathbf{v}_g + \mathbf{v}_a, \quad (3.5a)$$

where

$$\mathbf{v}_g = \frac{c_p\Theta_0}{f_0}\mathbf{k}\times\nabla\pi. \quad (3.5b)$$

Since the geostrophic part of the velocity is nondivergent, the geopotential flux term can be written as

$$-(c_p\Theta_0\nabla_3\cdot\mathbf{v}_3\pi) = -(c_p\Theta_0\nabla_3\cdot\mathbf{v}_a\pi). \quad (3.6)$$

In the evolution of the cyclone studied by OK, it was found that the export of energy by this ageostrophic geopotential flux was the primary reason for the decay of the cyclone. The exported energy then acted as input to the growth of a new disturbance downstream. The current study will examine, through use of a simple idealized model, the role played by this term in the development of baroclinic waves.

## 4. Results of linear experiments

### *a. Eady case on an f plane*

The evolution of the localized perturbation imposed on the Eady basic flow on an $f$ plane is depicted in Fig. 3, which shows the pressure field at 2-day intervals for 0.5-km altitude. As expected from a linear experiment, the growth of the disturbances is almost exponential in time. Because the steering velocity for this case is zero [for simplicity, we have taken a mean flow such that $U(H/2)$ equals 0 here], the waves develop without movement relative to the flow. Within three days, the initial perturbation (at the center of the channel) obtains, locally, the shape of the most unstable baroclinic normal mode. Notice that in time, other unstable eddies grow both upstream and downstream of the initial eddy. The evolution of the vertically in-

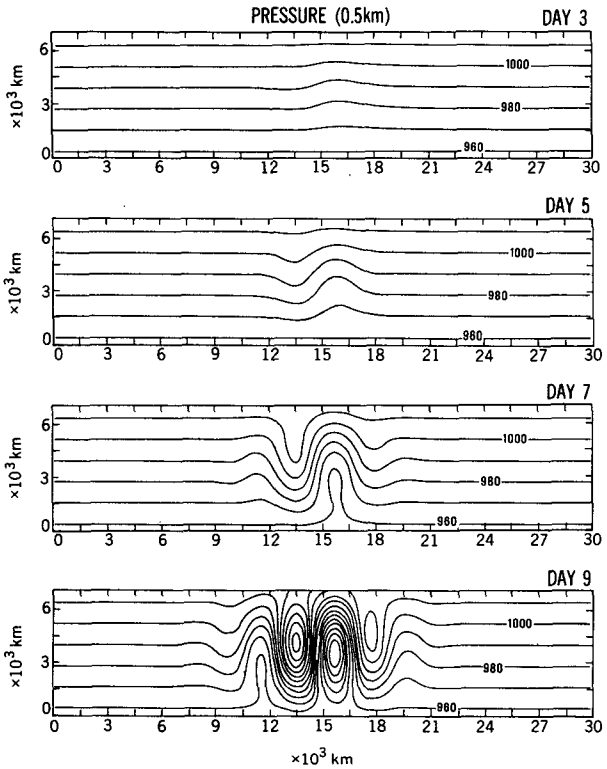


FIG. 3. Evolution of the pressure for the linear Eady experiment at lower level (0.5 km) for days 3, 5, 7, and 9.

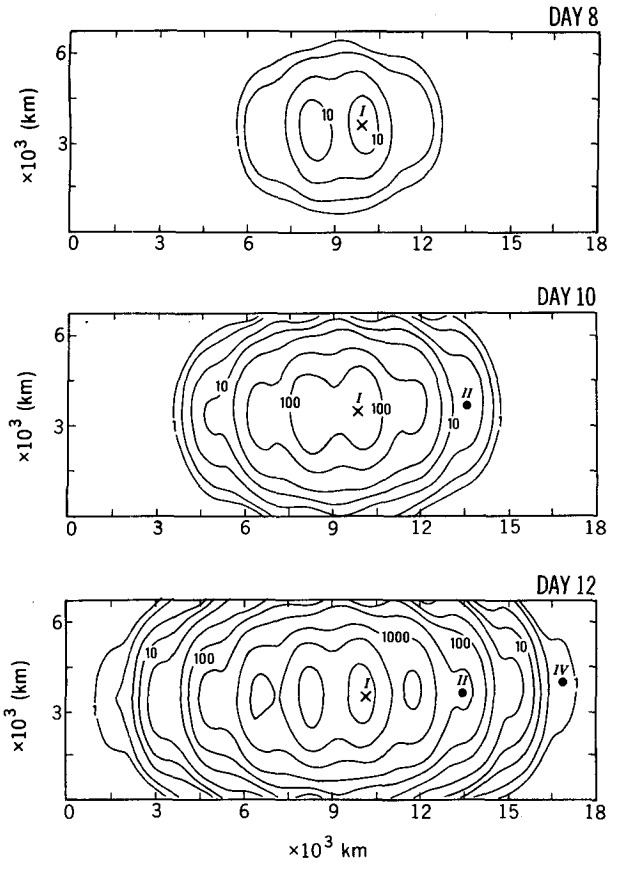


FIG. 4. Evolution of the vertically integrated eddy kinetic energy for the linear Eady flow. Note that only the central 18 000 km of the channel is shown. The crosses mark the position of the initial wave, and the dots labeled II and IV mark the positions of the second and fourth downstream waves, whose energetics will be shown in Fig. 5.

tegrated eddy kinetic energy over the middle part of the channel is shown in Fig. 4. The initial perturbation is marked by a cross (×). Figure 4 shows that by day 8, waves start to appear both upstream and downstream of the initial disturbance. By day 10, a second downstream wave (II), as well as an upstream wave, becomes apparent, with additional waves appearing later (IV). Since the waves are all stationary, the evolution of each wave can be examined by computing the energetics for a given area around the point of maximum energy for each wave packet. The result is shown in Fig. 5 for the initial wave as well as the second (II) and fourth (IV) downstream waves. Because of the symmetry of the basic state about the midlevel, evolution of the upstream waves is identical to that of the downstream waves, and their energetics are not shown here. The results shown in Fig. 5 are broken down into the total normalized growth rate ($A$), and its contributions from the ageostrophic flux divergence term ($B$), the baroclinic term ($C$), the advection term ($D$), and the barotropic conversion term ($E$) as defined from section 3:

$$\frac{\left[\frac{\partial}{\partial t}K_e\right]}{[K_e]} = A$$

$$\frac{[-(c_p\Theta_0\nabla_3\cdot v_a\pi)]}{[K_e]} = B$$

$$\frac{\left[g\frac{w}{\Theta_0}\theta\right]}{[K_e]} = C$$

$$\frac{\left[-\left(\bar{U}\frac{\partial}{\partial x}\right)K_e\right]}{[K_e]} = D$$

and

$$\frac{[-(\mathbf{v}\cdot(\mathbf{v}_3\cdot\nabla_3)\bar{\mathbf{V}})]}{[K_e]} = E. \tag{4.1}$$

The volume integral is defined by

$$[F] = \int_\Sigma \int_0^H F dz da, \tag{4.2}$$

where $\Sigma$ is the rectangular area that covers the entire width of the channel and encompasses one relative $K_e$ maximum, that is, from one $K_e$ minimum to the next minimum.

For the initial disturbance, the baroclinic term ($C$) is the dominant source of kinetic energy, while the ageostrophic flux term ($B$) represents the primary sink. With the baroclinic term dominating, the wave grows continuously. Since the simulation is linear, the magnitude of the baroclinic term cannot decrease and the wave continues to grow over the 20-day period of the experiment.

Note, however, that for the second downstream wave (II), the initial growth is dominated by the positive contribution from the ageostrophic flux term ($B$). (The terms "upstream" and "downstream" are defined as relative to the initial wave, with "downstream" referring to points east of the initial wave.) After approximately 10 days, the baroclinic conversion term ($C$) becomes significant, and by the end of the 20-day period the baroclinic term has become stronger. When the integration was continued for another 20 days (not shown), it was found that the wave evolution eventually approached that of the initial perturbation discussed before, with baroclinic conversion ($C$) dominating the growth and the primary energy-loss mechanism being the ageostrophic flux term ($B$).

The evolution of the fourth downstream wave (IV) is simply a delayed version of the second downstream wave (II). It is important to note that in the instances where the growth is dominated by the ageostrophic

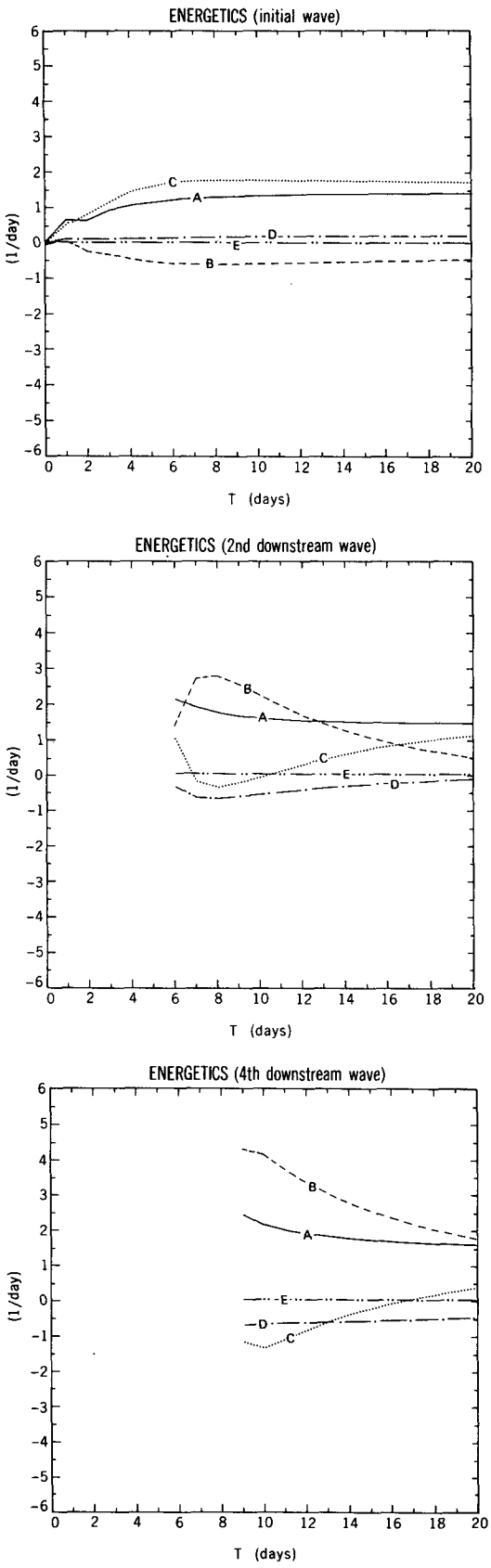


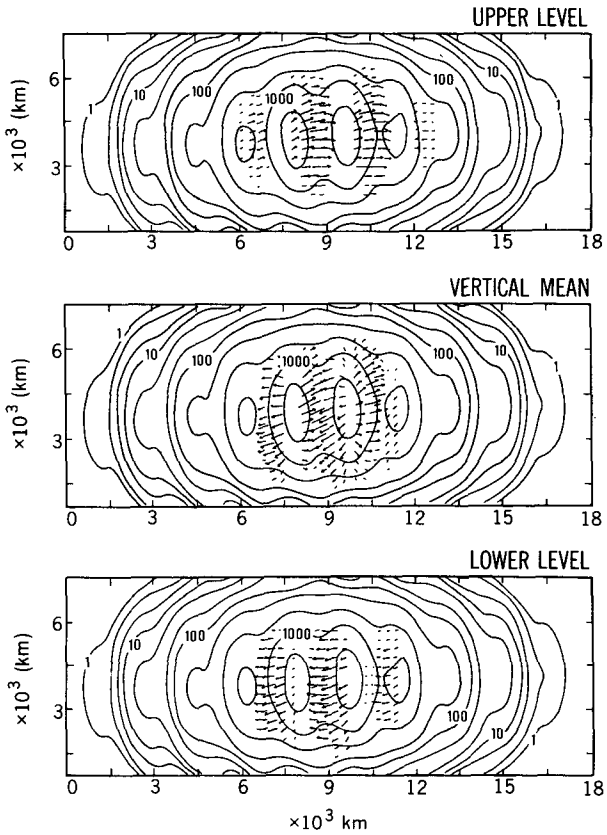


FIG. 6. The contours in the panels show the vertically integrated eddy kinetic energy at day 12 of the linear Eady experiment. The vectors denote the ageostrophic fluxes at the upper level (top panel), the lower level (bottom panel), and vertical mean ageostrophic fluxes (middle panel).

flux term ($B$), the growth rate can be higher than the normal-mode growth rate, in agreement with the results of SH. The preceding discussions imply that as the initial disturbance grows, it exports energy via the ageostrophic flux term both upstream and downstream, triggering the growth of other disturbances. This process repeats itself with these subsequent disturbances. Figure 6 shows the patterns of eddy kinetic energy and the ageostrophic fluxes at day 12 of the integration for two levels in the model. The upper-level (12.5 km) and lower-level (0.5 km) patterns are shown in the top and bottom panels, respectively. The vertically averaged fields are shown in the middle panel. It is evident from Fig. 6 that each wave packet is losing energy both upstream and downstream. With each successive disturbance developing later than the previous one, however,

FIG. 5. Energetics of the initial wave, the second downstream wave, and the fourth downstream wave of the linear Eady experiment. The positions of the waves are shown in Fig. 4. The curves $A$ to $E$ are as defined in (4.1).

the energy lost by the wave to the subsequent disturbance is less than the energy it gains from the previous disturbance, since the amplitude of the preceding disturbance is much larger. Hence, there is a net positive contribution to growth of each disturbance by the ageostrophic flux term, at least until the amplitude of the wave exceeds that of the preceding wave, at which time there will be a net loss of energy via the ageostrophic flux term.

These results are in general agreement with those of OK concerning the role of the ageostrophic fluxes. One difference, however, is that OK found predominantly *downstream* ageostrophic fluxes, while the results in the current study indicate fluxes in both the upstream and downstream directions. This difference has already been noted by SH. They also found both upstream and downstream development in their idealized calculations, but pointed out the rarity of upstream development in an observational study. Using the balance between the advection and stretching terms in the vorticity equation, OK argued that the ageostrophic fluxes will be predominantly downstream in the upper troposphere where the wave lags the mean flow. Analogous arguments imply that ageostrophic fluxes in the lower atmosphere will be predominantly upstream since the wave moves faster (in a relative sense) than the mean flow at that level. The results shown in Fig. 6 confirm that the fluxes are indeed predominantly upstream at lower levels and downstream at upper levels. The discrepancy between the current results and those of OK, in terms of the vertically averaged fluxes, can be explained by surface friction effects, which will tend to decrease the amplitude of the wave in the lower levels and reduce the upstream ageostrophic fluxes. Figure 7 shows a case in which a simple Rayleigh friction has been applied in the three lowest layers as a gross representation of the effects of surface friction. A drag coefficient of $(2\ \text{day})^{-1}$ is used for the lowest level, with the drag decreasing linearly to zero at the fourth level. It can be seen that, while both the upstream and downstream disturbances are weakened, the upstream developments have been weakened to a much greater extent.

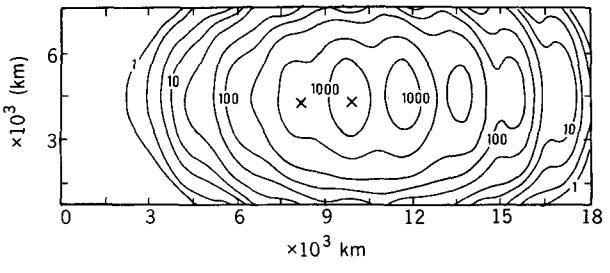


FIG. 7. Vertically integrated eddy kinetic energy at day 12 of the linear Eady experiment with a Rayleigh-type surface friction at the lowest three levels. This should be compared with the bottom panel of Fig. 4, which shows the corresponding values for the Eady experiment without surface friction. The crosses mark the positions of the initial disturbances.

Another question that one may ask is which part of the wave spectrum is responsible for the propagation of energy. Here (and also in SH) it was found that the downstream disturbances first appear at the upper level and develop downwards, while the upstream disturbances first appear near the ground and develop upwards. Since, for the Eady problem, the unstable modes have a structure that extends throughout the entire depth of the atmosphere, one may expect that the neutral modes are important in the propagation of energy and the triggering of growth downstream (and upstream). This question was addressed by performing an eigenvalue analysis of the quasigeostrophic Eady problem. Eigenmodes of the two-dimensional Eady problem were found, and an initially localized barotropic disturbance was subjected to a Fourier analysis and projected onto these eigenmodes. The procedure is very similar to that used by Farrell (1982), who concentrated on short time response (less than ~2 days). In this case, however, we are more interested in the longer time response. An example of the evolution of these eigenmodes, after 11 days, is shown in Fig. 8a, and the results are similar to those found by integration of the primitive equation. Figure 8b shows the result when only the initial perturbation is projected onto the unstable Eady modes, and all neutral modes are taken out. The results are very similar to those shown in Fig. 8a, with the only difference appearing in the very short waves at the leading edge of the packet. What can be said in terms of the eigenmodes is that the Eady unstable modes of different wavelengths interfere with each other and, while each mode is "symmetric" about the midplane, the different vertical phase tilt of each mode yields a combined vertical structure of many modes that need not be symmetric about the midplane, particularly at the leading edges. Thus, it is the unstable mode that contributes to the energy fluxes since, for a linear experiment, the amplitude of the neutral waves can be made arbitrarily small by starting the integration with an arbitrarily small perturbation, and the neutral waves can never affect the (long time) dynamics of the problem.

### *b. The jet basic flow on an f plane*

The linear initial-value problem for the case of a westerly jet basic state was also examined using the numerical model. Results of the experiments are, in general, very similar to those for the Eady case. (Here, we have chosen a jet whose half-width is greater than the radius of deformation; thus, the evolution is mainly baroclinic rather than barotropic. See, for example, Feldstein 1991.) Figure 9 shows the energetics for both the initial (Fig. 9a) and the fourth downstream perturbations (Fig. 9b), in a frame of reference that follows the wave packets. An extra term that comes into the

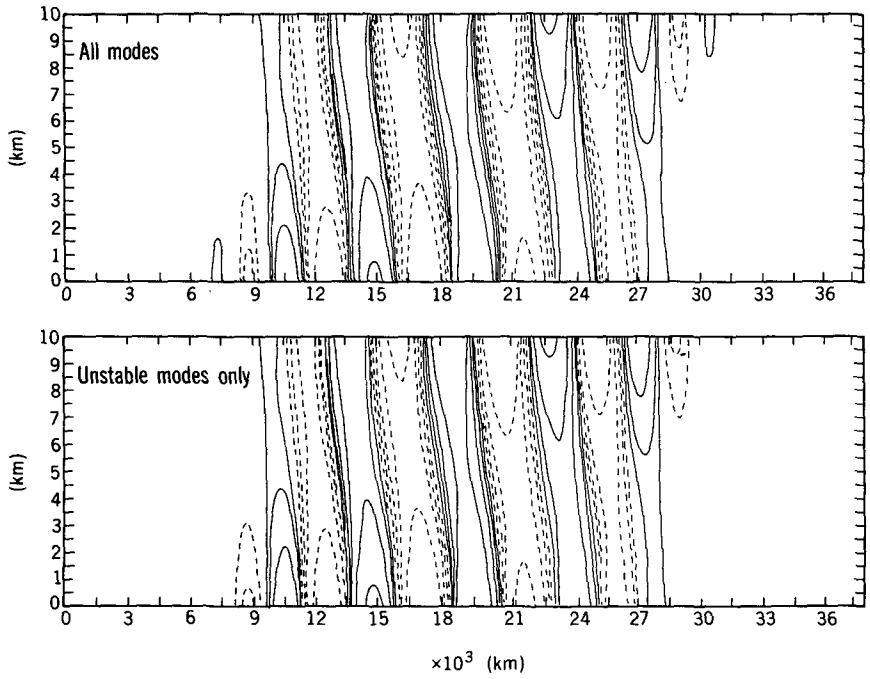


FIG. 8. Streamfunction on day 11 of two-dimensional initial-value Eady problem with a localized initial disturbance. Upper panel: Complete solution. Lower panel: Projection of solution on unstable Eady modes only with amplitudes of neutral or decaying modes set to zero.

analysis due to the movement of the reference frame at the phase speed of the wave is shown combined with the advection term, since the two terms largely oppose each other. We see that the final growth rate is again dominated by the baroclinic term ($C$) and the ageostrophic flux term ($B$). As in the Eady case, the baroclinic term contributes to most of the growth of the initial disturbance, and the wave loses energy primarily via the ageostrophic flux term. For the fourth downstream wave, the growth is initially dominated by the advection ($D$) and ageostrophic flux terms ($B$), with the baroclinic term ($C$) becoming significant only later in the wave development. Again it was found that without surface friction, upstream and downstream developments are roughly symmetric.

### c. *Effects of beta*

The experiment involving the Eady basic flow was repeated for the case of a $\beta$ plane with $\beta = 1 \times 10^{-11}$ m$^{-1}$ s$^{-1}$. The same basic wind field was used, but the temperature field was modified to account for the effects of $\beta$. The distribution of eddy kinetic energy on day 12 is shown in Fig. 10. Since $\beta$ effectively reduces the phase speeds of the waves, the initial wave has moved to the left of the center of the channel, but both upstream and downstream developments are still evident. There now appears to be an asymmetry between the upstream and downstream developments, however, with the downstream ones being much stronger than the upstream ones. Similar results are also found for the jet case (not shown).

To understand the effects of beta in the asymmetry of upstream and downstream ageostrophic fluxes, let us inspect the linear quasigeostrophic meridional momentum equation:

$$f_0 u_a = -(\bar{U} - c)\frac{\partial v_g}{\partial x} - \beta y u_g. \qquad (4.3)$$

Here we have ignored the contribution from the growth of the wave, and $c$ is the phase speed of the wave. We only examine the equation for $u_a$ since the alongstream component of the fluxes is the more important one in the dispersion of energy (at least for the linear case). On an $f$ plane where $\beta$ is zero, the ageostrophic wind is antisymmetric (in $z$) about the midplane due to the change in sign of $\bar{U} - c$; $\beta$ introduces an additional term but also affects the ageostrophic flow by lowering the steering level of the wave, thus reducing $c$ (westward tendencies). Without loss of generality, let us just look at the changes in $u_a$ in the neighborhood of the central latitude, where $u_a$ has the maximum amplitude. (A more detailed analysis of the ageostrophic flow can be found in Lim et al. 1991.) Here, since $y \sim 0$, the main effect is due to the decrease in $c$, with the magnitude of $\bar{U} - c$ increasing in the upper levels and decreasing in the lower levels. Hence, $u_a$ is increased in the upper level and decreased in the lower level, thereby

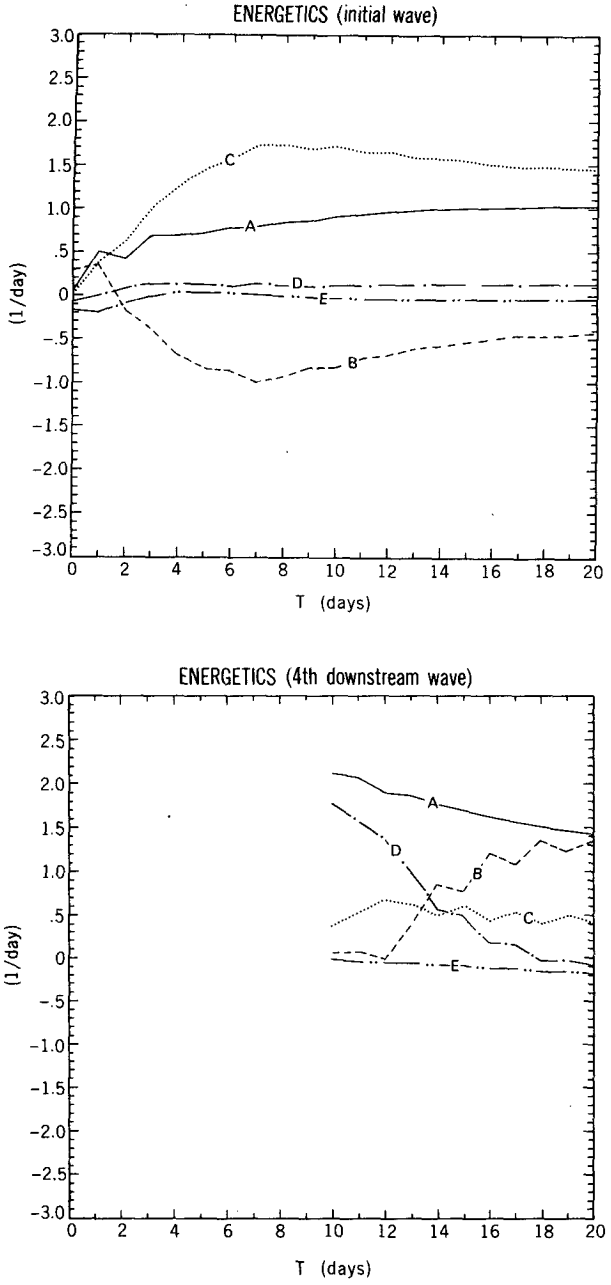


FIG. 9. Energetics of the initial wave and the fourth downstream wave of the linear solution with the jet basic state. The curves $A$ to $E$ are as defined in (4.1).

strengthening the ageostrophic fluxes in the upper levels and weakening them in the lower levels.

As shown in Fig. 6, the ageostrophic fluxes in the upper level point predominantly toward the downstream direction, while fluxes in the lower level point upstream. Thus, $\beta$ will lead to an increase in downstream fluxes and decrease in upstream fluxes, hence favoring downstream development over upstream development. We have computed the ageostrophic fluxes for the case on the beta plane (not shown), and indeed, the fluxes are predominantly downstream with only very weak upstream fluxes. The effect of $\beta$, together with surface friction, can largely explain why, observationally, predominantly downstream development is found, in agreement with OK.

## 5. Results of nonlinear experiments

A nonlinear run was performed with the jet case on the $\beta$ plane to examine the effects of nonlinearity. The evolution of the pressure field for the upper (right panels) and lower (left panels) levels is shown in Fig. 11 for days 10, 12, and 14. Comparing these results to that of the linear case (Fig. 3), we see that the nonlinearity has considerably modified the structure of the waves. At low levels, the lows (highs) are shifted poleward (equatorward) of the jet. Figure 12 shows the vertically averaged ageostrophic fluxes, flux divergence, and eddy kinetic energy at day 12 in a subregion comprising the most active area of development. (To enhance the divergent part of the ageostrophic fluxes, a nondivergent component equal to $0.2 * \mathbf{V}_g\Phi$ has been removed.) Note the clear pattern of ageostrophic flux convergence upstream of the eddy kinetic energy maximum and divergence downstream. As discussed in OK, flow particles gain energy upstream of the energy maximum due to the convergence of fluxes, reach a maximum, and then lose energy downstream.

The growth rate terms as defined in (4.1) were computed for an area of integration that follows the center of the wave packets. Because of nonlinear advection in this case, however, the two wave packets comprising a single cyclone interact with each other and become difficult to separate after some time (e.g., see Fig. 12). Hence, the energetics has been computed by combining both wave packets (i.e., roughly following the cyclone centers). The energetics for the initial, second downstream, and third downstream cyclones (O, P, Q of Fig. 11) are shown in Fig. 13. The primary difference between this case and the results of the linear experiments described in section 4 are that, because of the nonlinear interactions, the waves eventually stop growing. Closer examination of the energetics reveals

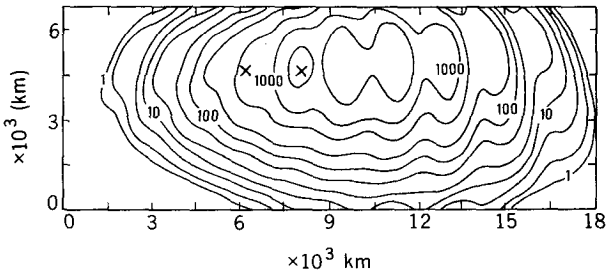


FIG. 10. Vertically integrated eddy kinetic energy at day 12 of the linear "Eady" experiment on a $\beta$ channel. The crosses mark the positions of the initial disturbances.

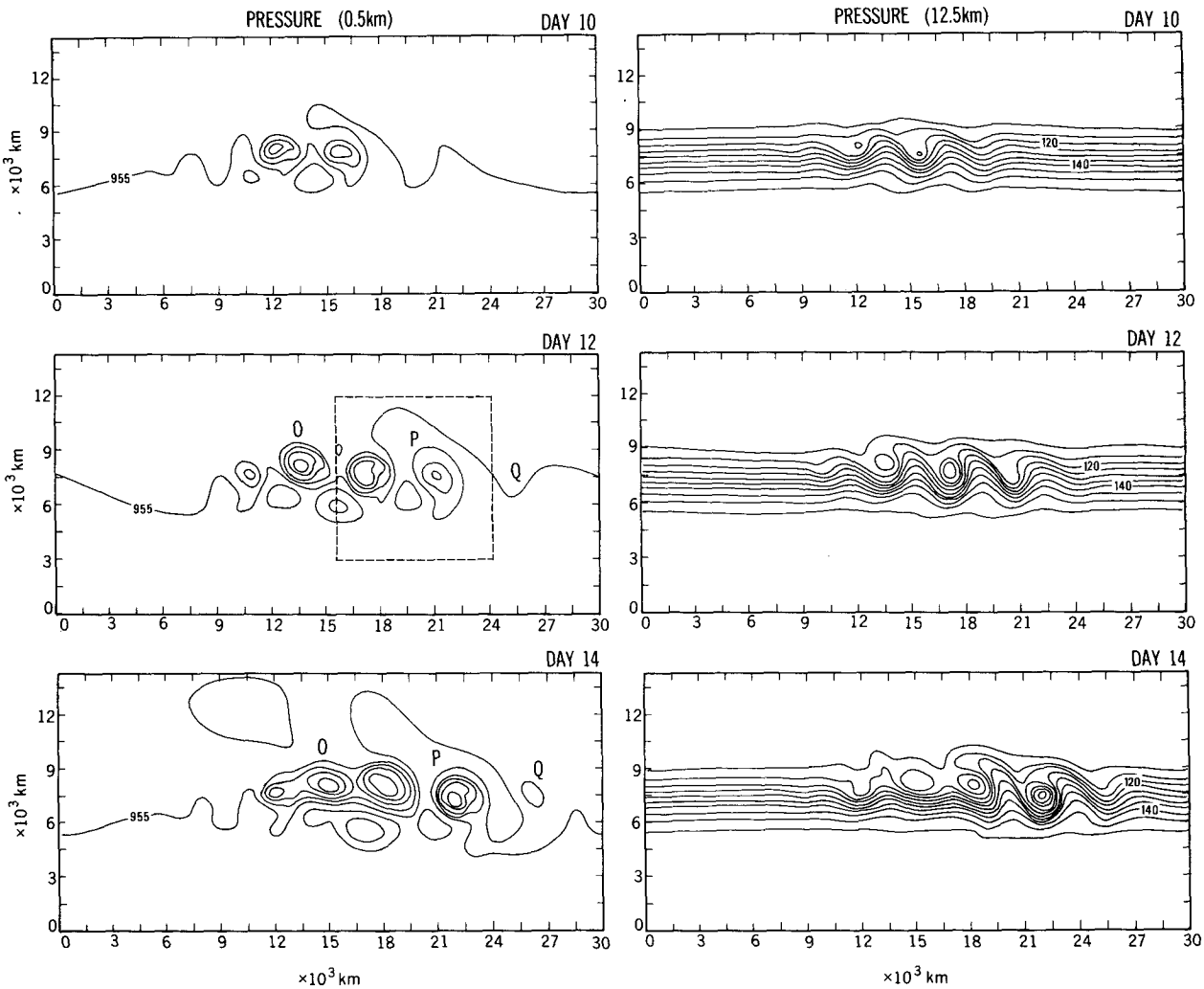


FIG. 11. Evolution of the pressure for the nonlinear solution with the jet basic state at 0.5 km (left panels) and 12.5 km (right panels). O, P, and Q mark the positions of the initial cyclone, the second downstream cyclone, and the third downstream cyclone, respectively, whose energetics will be shown in Fig. 13. The boxed area in the middle left panel marks the area to be shown in Fig. 12.

that while the growth of the initial wave is dominated by the baroclinic conversion term ($C$), early growth of the downstream waves is dominated by the ageostrophic flux convergence ($B$). Baroclinic conversion does not become dominant until the net growth rate of the wave has already peaked. The waves do eventually stop growing due to the decrease in baroclinicity, but the amplitudes of the waves do not actually decrease. This appears to be in conflict with earlier findings of life-cycle experiments (e.g., Simmons and Hoskins 1978) that nonlinear waves have a life cycle of baroclinic growth followed by barotropic decay. Here it appears that the barotropic conversion is entirely unimportant. This is because we have taken the perturbation to be deviations from the initial basic state, thus eliminating the changes of basic-state kinetic energy by the eddies, whereas in most normal-mode studies, the perturbations are taken to be deviations from the zonal-mean state, which is changing in time. We chose this approach in order to compare our results with those of the linear runs, and also because of the difficulties in defining a meaningful zonal-mean basic state, since the waves in different parts of the long channel are at widely different stages in their evolution and a zonal mean is not representative of the basic state seen by any particular wave. Hence, this study is drawing conclusions from only the initial stages of wave growth (at which stage the energetics should not be significantly affected by the choice of the basic state), and the results here support the findings of the linear studies that the growth of downstream (and upstream) waves are triggered by the ageostrophic fluxes that export energy from existing waves.

In the analysis of OK, which treated the time mean

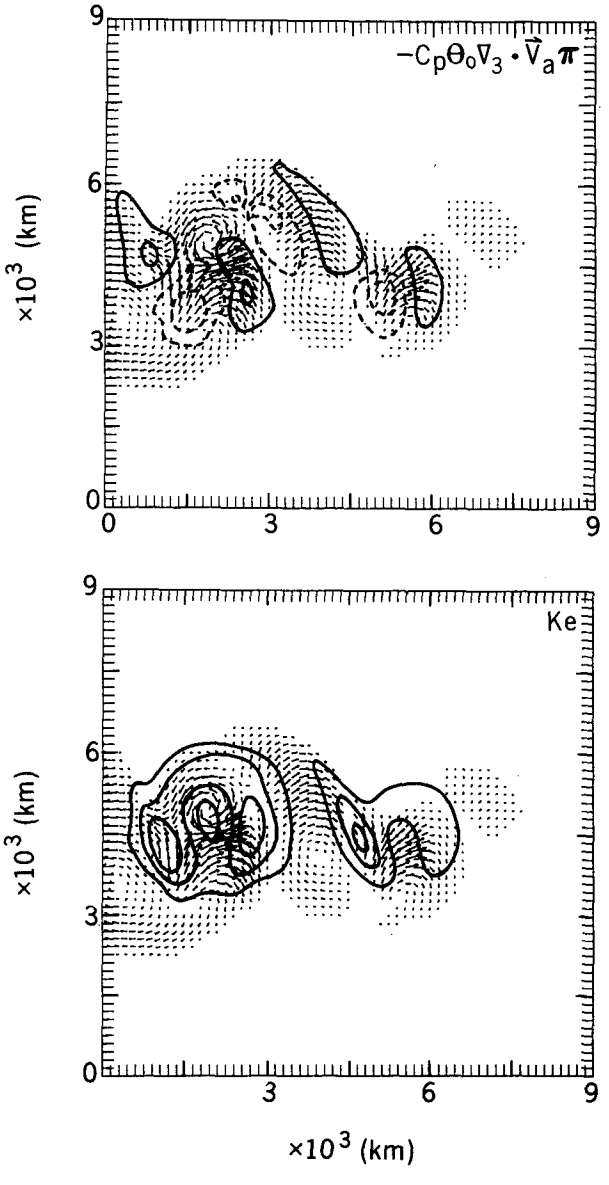


FIG. 12. The vectors show the ageostrophic fluxes on day 12 of the nonlinear solution with the jet basic state. The contours in the upper panel shows the vertically integrated divergence of the ageostrophic fluxes, with convergence shown by solid lines and divergence by dashed contours. The contours in the lower panel show the vertically integrated eddy kinetic energy. The area shown is marked out in the middle left panel of Fig. 11.

as the basic state, it was found that the barotropic conversion for each single wave packet was small compared with the ageostrophic fluxes. Their conjecture was that the individual energy packets of the normal modes would exhibit ageostrophic flux divergence with magnitudes exceeding that of the barotropic conversion. Zonally averaged, the effects of the ageostrophic fluxes for individual packets should cancel, with the net effect being a sink of eddy energy via barotropic conversion and a source via baroclinic conversion, as was found in Simmons and Hoskins (1978). Locally, however, ageostrophic fluxes are important in the energy life cycle of an individual normal mode. In other experiments with normal-mode growth we have found that the amplitudes of the ageostrophic flux divergence can be as large as or even larger than that of the baroclinic conversion terms. Because of the exact periodicity of single normal modes, however, the positive contributions by fluxes from upstream are exactly balanced by the fluxes radiated downstream, and the net integrated flux contribution is zero.

## 6. Absolute and convective instabilities

Merkine (1977) introduced the mathematical framework for treating absolute versus convective instabilities into the field of meteorology. A brief discussion on the convective or absolute characteristics of the Eady problem can be found in SH. Their conclusion, which was based on an asymptotic expansion solution, was that an observer moving with a speed, $V_{obs}$, between the maximum and minimum flow speeds will witness an exponential instability, basically:

$$U_{min} < V_{obs} < U_{max}. \tag{6.1}$$

Then, if $U_{min} < 0$, the Eady problem will be absolutely unstable. Similar discussions for the Charney (1947) baroclinic instability problem can be found in Pierrehumbert (1986). A recent review of local and global instabilities can be found in Huerre and Monkewitz (1990).

In this section, we will attempt to treat the problem in a more physical manner. Orlanski and Katzfey defined a relative group velocity in terms of the ageostrophic fluxes by dividing the volume integral of the ageostrophic fluxes by the integral of the total eddy energy. Since in the energy equation (3.3), the ageostrophic fluxes and the advective fluxes are the only energy transport terms, we expect physically that these fluxes should be related to the rate that an unstable wave packet spreads out. Following OK, we can define a relative group velocity as

$$\mathbf{C}_{gR} = \frac{\iint (c_p\Theta_0\mathbf{v}_a\pi)\,dzdA}{\iint \mathrm{TE}_e\,dzdA}, \tag{6.2}$$

where $\mathrm{TE}_e$ is the total perturbation energy (kinetic plus potential). Energy is also transported by the flow. Similarly, then, the total group velocity could be defined as follows:

$$\mathbf{C}_{gT} = \frac{\iint (c_p\Theta_0\mathbf{v}_a\pi + \mathrm{TE}_e\mathbf{V})\,dzdA}{\iint \mathrm{TE}_e\,dzdA}. \tag{6.3}$$

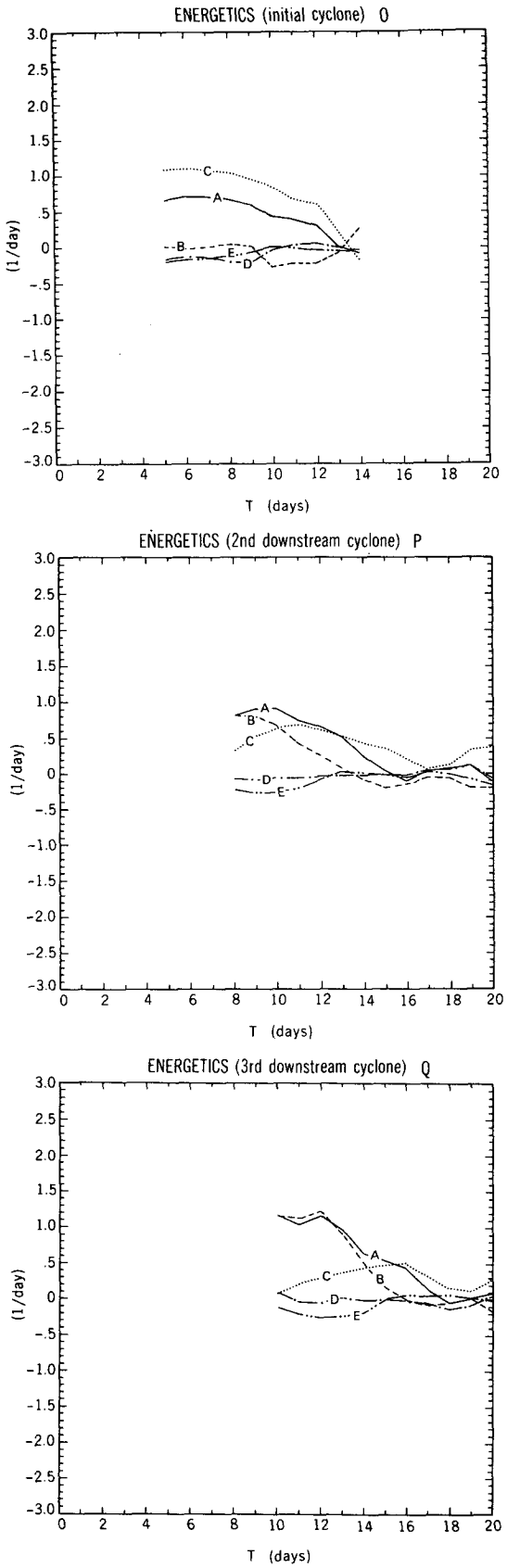


FIG. 13. Energetics of the initial cyclone, the second downstream cyclone, and the third downstream cyclone (O, P, and Q, respectively) of the nonlinear solution with the jet basic state. The positions of the cyclones are shown in Fig. 11. The curves $A$ to $E$ are as defined in (4.1).

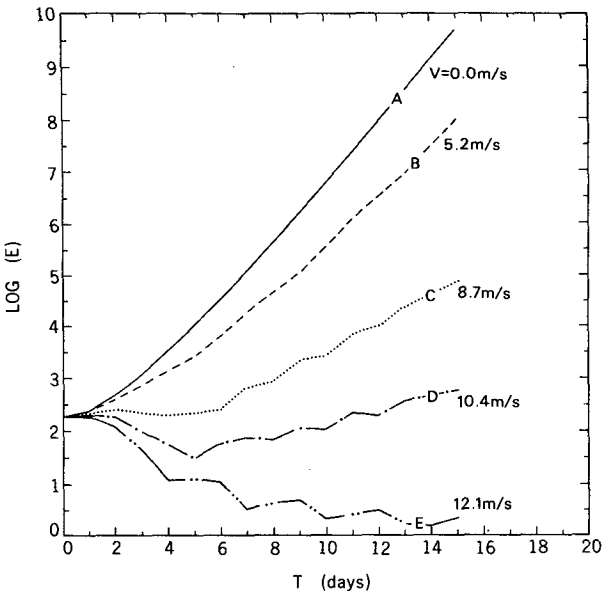


FIG. 14. Evolution of the volume-integrated eddy kinetic energy for the linear Eady experiment as seen by observers moving with different velocities $V$.

The quantity $\mathbf{C}_{gT}$ can be interpreted as the velocity at which the energy of the wave packet is being transported by both the flow and the ageostrophic fluxes. For the linear cases, $\bar{U}$ takes the place of $\mathbf{V}$ in (6.3). In some limiting cases such as that of small-amplitude Rossby waves, this expression leads to the group velocity (Pedlosky 1979). It should be pointed out that the energy equation [(3.3) and (3.4)] depends on the divergence of the fluxes and not on the fluxes themselves. While any nondivergent vector added to the ageostrophic fluxes will not change the energy budget, it could introduce considerable ambiguity to (6.3). However, since the definition of group velocity is meaningful only when the integral in (6.3) is taken over multiples of half-wavelengths, it turns out that even if we had taken the total perturbation velocity $\mathbf{v}_3$ instead of $\mathbf{v}_a$ in (6.3), the resulting $\mathbf{C}_{gT}$ comes out to be exactly the same due to the fact that the integral of $\mathbf{v}_g \pi$ vanishes over one-half wavelength. Hence, this definition is not really ambiguous.

Now let us restrict ourselves to discussion of the Eady problem, the dynamics of which is invariant under a Galilean transformation. The solution for this case has been discussed in detail in section 4a. Figure 14 shows the evolution of the total energy computed in a frame

of reference moving downstream from the initial disturbance at a constant velocity. The different curves show the energy for frames moving at different speeds, averaged over a volume occupying the entire width of the channel and having a length of a half-wavelength of the waves. The basic state for this case does not have a barotropic component, so the initial disturbance will remain stationary. The curve labeled with zero velocity shows the evolution of the initial disturbance. We see that as the speed of movement of the frame is increased, the growth rate of the total energy decreases, and finally when the speed approaches 11 m $s^{-1}$, the energy actually decreases with time. The total group velocity as defined by (6.3) was calculated for the entire channel (see Fig. 15), again averaged over a half-wavelength. The total group velocity as defined by (6.3) is shown by the solid curve, and the contribution from the advection part is shown by the dashed curve. The difference between the two curves represents the contribution by the ageostrophic fluxes (6.2). It can be seen that for this case, the ageostrophic fluxes contribute to about half of the total amplitude of the total group velocity. It was found that the maximum group velocity occurs near the leading edge of the spreading wave packet and is also about 11 m $s^{-1}$ when averaged over days 5 to 15. Figure 16 shows the average growth rate observed from frames moving with different velocities. In the period between days 5 and 15, we again see that the growth rate becomes zero at approximately $V \approx 11$ m $s^{-1}$, indicating that the packet is spreading out with a speed of about 11 m $s^{-1}$. The preceding results suggest that if the speed of the frame is higher than the maximum group velocity, the energy seen by the observer will decrease, whereas if the speed is lower than the maximum group velocity, the energy will increase.

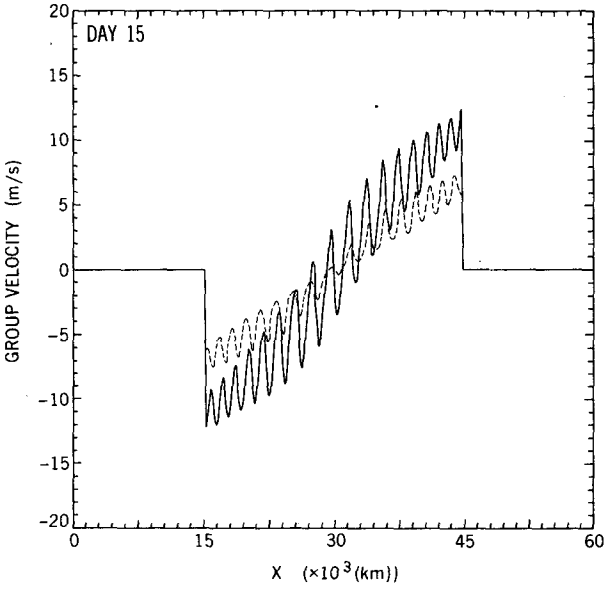


FIG. 15. Solid curve: The total group velocity as defined by (6.3) for the linear Eady experiment plotted against the length of the channel for the solution on day 15. Dashed curve: Contribution to the total group velocity by the advection part. Note that the total channel length is doubled (60 000 km) for this case in order that the leading fringes on the two sides will not interfere with each other.

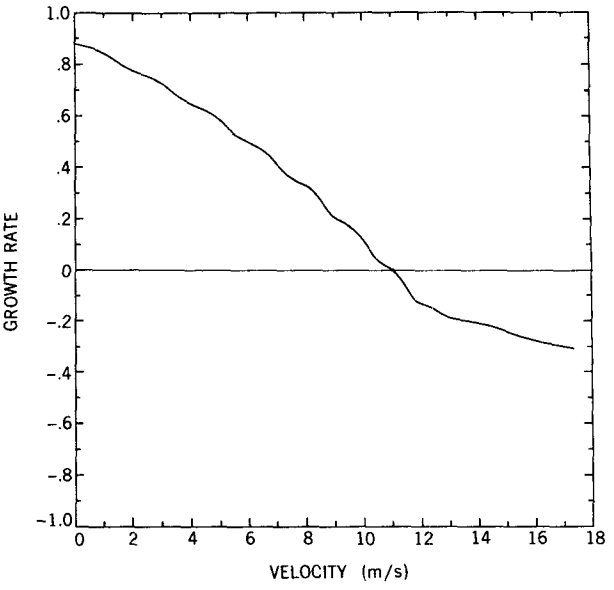


FIG. 16. The average growth rate for the solution of the linear Eady experiment between days 5 and 15 observed from frames moving with different velocities.

Now we translate the problem to a situation where the basic flow has a nonzero westerly barotropic component. Here, the energy of the wave packet is being advected downstream (toward the east) by the basic flow. However, there is also energy transport both upstream and downstream due to the ageostrophic geopotential fluxes. The results presented suggest that if the total minimum group velocity is always positive, the energy of the disturbance will decrease eventually if we are at a fixed point. This case corresponds to the case of convective instability. If the basic westerly flow is not too strong, however, there is a possibility that the upstream ageostrophic geopotential fluxes can overcome the effects of the advection by the basic flow, and the total group velocity can become negative for an observer at a fixed location. Even after the maximum of the wave packet has passed, since there is a constant inflow of energy from downstream, the disturbance will continue to grow indefinitely, corresponding to the case of absolute instability. We can summarize the absolute or convective instability condition by requiring that

$$(C_{gT})_{\min} < 0 < (C_{gT})_{\max} \quad \text{absolute instability}$$

$$0 < (C_{gT})_{\min} < (C_{gT})_{\max} \quad \text{convective instability,} \quad (6.4)$$

where $C_{gT}$ is as defined in (6.3). Similar results have been obtained for the jet case as well as the $\beta$-plane case.

## 7. Conclusions

It has been shown that ageostrophic geopotential fluxes contribute significantly to the upstream and downstream developments of baroclinic waves. Fluxes radiated from an existing large-amplitude wave have been found to lead to growth of downstream waves. This is consistent with the results of an earlier case study in which it was also demonstrated that radiation of fluxes downstream were primarily responsible for the decay of the wave under analysis. The findings of the current study have also been useful in understanding features such as the rapid growth of, and the asymmetry between, upstream and downstream wave development.

The relationship between the ageostrophic fluxes and the rate of spreading of a localized wave packet has also been investigated. A group velocity has been defined that includes both the advective flux and the ageostrophic fluxes, and it has been suggested that it is this group velocity that governs the speed at which the packet spreads upstream and downstream. It has also been demonstrated that the long-term evolution of unstable wave packets is governed primarily by the evolution of the most unstable waves, with neutral modes modifying the final solution only slightly.

The linear solutions discussed in section 4 and the solutions presented in SH all correspond to an ever-expanding pulse eventually taking over the whole domain. This seems to be at odds with observations, which hardly ever show such occurrences. In order to compare with observations, we expect that fully nonlinear solutions have to be considered. Here we have discussed only briefly the effects of nonlinearity in section 5. Lee (1991) found coherent wave packets in the Southern Hemisphere using ECMWF data, and the existence of these wave packets is closely related to downstream development. In an upcoming paper, we will examine the dynamics of a midlatitude storm track using the ideas of downstream development discussed in this paper.

A natural question to ask is whether the ideas presented in this study suggest that analysis of ageostrophic fields in synoptic data could help to pinpoint positions of future cyclone developments. Orlanski and Katzfey showed that the effects were important for a real case in the southern Pacific, and one would expect similar events to occur in the Northern Hemisphere, as well. Of course, other effects such as the background environment, orography, and surface effects all influence the developments of storms, and the generality of the results obtained here will require further study.

*Acknowledgments.* The authors would like to thank Dr. I. Held for his valuable comments and suggestions; Mr. J. Sheldon, Dr. B. Gross, Dr. J. Mahlman, and Dr. R. Pierrehumbert for editorial comments that clarified this paper; and Phil Tunison and the GFDL drafting department for their assistance in preparing the figures. One of the authors (EC) is supported by NSF Grant ATM 8800667.

## REFERENCES

Charney, J. G., 1947: The dynamics of long waves in a baroclinic westerly current. *J. Meteor.*, **4**, 135–162.

Eady, E. T., 1949: Long waves and cyclone waves. *Tellus*, **1**, 33–52.

Farrell, B., 1982: The initial growth of disturbances in a baroclinic flow. *J. Atmos. Sci.*, **39**, 1663–1686.

——, 1984: Modal and nonmodal baroclinic waves. *J. Atmos. Sci.*, **41**, 668–673.

Feldstein, S. B., 1991: A comparison of the weakly nonlinear instability of westerly and easterly jets in a two-layer beta-plane model. *J. Atmos. Sci.*, **48**, 1701–1717.

Huerre, P., and Monkewitz, P. A., 1990: Local and global instabilities in spatially developing flows. *Ann. Rev. Fluid Mech.*, **22**, 473–537.

Lee, S., 1991: Baroclinic wave packets in models and observations. Ph.D. dissertation, Princeton University, 214 pp.

Lim, G. H., J. R. Holton, and J. M. Wallace, 1991: The structure of the ageostrophic wind field in baroclinic waves. *J. Atmos. Sci.*, **48**, 1733–1745.

Merkine, L., 1977: Convective and absolute instability of baroclinic eddies. *Geophys. Astrophys. Fluid Dyn.*, **9**, 129–157.

Nakamura, N., 1989: Dynamics of baroclinic instability in rapid cyclogenesis. Ph.D. dissertation, Princeton University, 150 pp.

Orlanski, I., and J. Katzfey, 1991: The life cycle of a cyclone wave in the Southern Hemisphere. Part I: Eddy energy budget. *J. Atmos. Sci.*, **48**, 1972–1998.

Pedlosky, J., 1979: *Geophysical Fluid Dynamics.* Springer, 624 pp.

Pierrehumbert, R. T., 1986: Spatially amplifying modes of the Charney baroclinic-instability problem. *J. Fluid Mech.*, **170**, 293–317.

Ross, B. B., and I. Orlanski, 1982: The evolution of an observed cold front. Part I: Numerical simulation. *J. Atmos. Sci.*, **39**, 296–327.

Simmons, A. J., and B. J. Hoskins, 1978: The life cycles of some nonlinear baroclinic waves. *J. Atmos. Sci.*, **35**, 414–432.

——, and ——, 1979: The downstream and upstream development of unstable baroclinic waves. *J. Atmos. Sci.*, **36**, 1239–1254.